The Plant Cell, Vol. 32: 2491–2507, August 2020, www.plantcell.org © 2020 ASPB.

Coordinated Activation of ARF1 GTPases by ARF-GEF GNOM Dimers Is Essential for Vesicle Trafficking in Arabidopsis

Sabine Brumm,[a] Manoj K. Singh,[a] Mads Eggert Nielsen,[a,b] Sandra Richter,[a] Hauke Beckmann,[a] York-Dieter Stierhof,[c] Angela-Melanie Fischer,[a] Mande Kumaran,[d] Venkatesan Sundaresan,[e] and Gerd Jürgens[a,1]

[a] Center for Plant Molecular Biology, Developmental Genetics, University of Tübingen, 72076 Tübingen, Germany
[b] University of Copenhagen, Faculty of Science, Section for Plant and Soil Science, 1871 Frederiksberg C, Denmark
[c] Center for Plant Molecular Biology, Microscopy, University of Tübingen, 72076 Tübingen, Germany
[d] Temasek Life Sciences Laboratory, National University of Singapore, 117604 Singapore
[e] Department of Plant Biology and Department of Plant Sciences, University of California, Davis, California 95616

ORCID IDs: 0000-0003-1498-3880 (S.B.); 0000-0003-0197-6876 (M.K.S.); 0000-0001-6170-8836 (M.E.N.); 0000-0001-7765-5759 (S.R.); 0000-0003-0277-8556 (H.B.); 0000-0002-1784-1768 (Y.-D.S.); 0000-0002-9600-2646 (A.-M.F.); 0000-0002-6452-7624 (M.K.); 0000-0002-4670-0630 (V.S.); 0000-0003-4666-8308 (G.J.)

Membrane trafficking maintains the organization of the eukaryotic cell and delivers cargo proteins to their subcellular destinations, such as sites of action or degradation. The formation of membrane vesicles requires the activation of the ADP-ribosylation factor ARF GTPase by the SEC7 domain of ARF guanine-nucleotide exchange factors (ARF-GEFs), resulting in the recruitment of coat proteins by GTP-bound ARFs. In vitro exchange assays were done with monomeric proteins, although ARF-GEFs form dimers in vivo. This feature is conserved across eukaryotes, although its biological significance is unknown. Here, we demonstrate the proximity of ARF1●GTPs in vivo by fluorescence resonance energy transfer-fluorescence lifetime imaging microscopy, mediated through coordinated activation by dimers of Arabidopsis (*Arabidopsis thaliana*) ARF-GEF GNOM, which is involved in polar recycling of the auxin transporter PIN-FORMED1. Mutational disruption of ARF1 spacing interfered with ARF1-dependent trafficking but not with coat protein recruitment. A mutation impairing the interaction of one of the two SEC7 domains of the GNOM ARF-GEF dimer with its ARF1 substrate reduced the efficiency of coordinated ARF1 activation. Our results suggest a model of coordinated activation-dependent membrane insertion of ARF1●GTP molecules required for coated membrane vesicle formation. Considering the evolutionary conservation of ARFs and ARF-GEFs, this initial regulatory step of membrane trafficking might well occur in eukaryotes in general.

INTRODUCTION

Activation of the small GTPase ARF1 by guanine-nucleotide exchange factors (ARF-GEFs) plays a pivotal role in membrane traffic across eukaryotes (Donaldson and Jackson, 2011). GDP-bound ARF1 interacts with the catalytic SEC7 domain of ARF-GEFs on donor membranes, resulting in GDP-GTP exchange on ARF1 and the insertion of its myristoylated N-terminal hasp into the membrane (Casanova, 2007; Anders and Jürgens, 2008; Bui et al., 2009). GTP-bound ARF1 interacts with coat proteins involved in vesicle formation and cargo recruitment (D'Souza-Schorey and Chavrier, 2006; Gillingham and Munro, 2007; Singh and Jürgens, 2018). In vitro studies revealed the formation, in a cross-linker-dependent fashion, of ARF1●GTP dimers that are required for the scission of membrane vesicles from donor membranes (Beck et al., 2008, 2011). ARF1 dimer formation was disrupted by the Tyr-35-to-Ala (Y35A) substitution, which reduced the yield of vesicle formation dramatically in vitro and failed to complement the lethality of the *arf1 arf2* double mutant in yeast (*Saccharomyces cerevisiae*), carrying deletions in the two yeast Arf1 paralogs (Beck et al., 2008). The vesicle scission defects observed in vitro were largely overcome by chemical cross-linking of ARF1-Y35A variants (Beck et al., 2011). Whether or not ARF1 dimers exist in vivo and how they might form has however not been addressed. In this context, it might be relevant to consider the role of ARF-GEFs in ARF1 activation. Large ARF-GEFs such as human Golgi-specific brefeldin A-resistance factor1 (GBF1) or Arabidopsis (*Arabidopsis thaliana*) GNOM have a stereotypic domain organization, including an N-terminal dimerization (DCB) domain (Casanova, 2007; Anders et al., 2008; Bui et al., 2009). The DCB domain can interact with another DCB domain and with at least one other ARF-GEF domain (Grebe et al., 2000; Ramaen et al., 2007; Anders et al., 2008). Although conserved across eukaryotes, the biological significance of ARF-GEF dimerization is not known. Our results presented here suggest that ARF-GEF dimers generate ARF1●GTP proteins spaced in close proximity on the target membrane during the activation process, promoting productive vesicle formation.

RESULTS AND DISCUSSION

In Vivo Occurrence and Biological Significance of Closely Spaced ARF1 GTPases

We tested wild-type ARF1 (ARF1A1C; gene identifier At2g47170) and two ARF1 variants, the activation-deficient ARF1-T31N and

[1] Address correspondence to gerd.juergens@zmbp.uni-tuebingen.de. The author responsible for distribution of materials integral to the findings presented in this article in accordance with the policy described in the Instructions for Authors (www.plantcell.org) is: Gerd Jürgens (gerd.juergens@zmbp.uni-tuebingen.de).
www.plantcell.org/cgi/doi/10.1105/tpc.20.00240

IN A NUTSHELL

Background: Eukaryotic cells deliver one out of every three proteins to their sites of action (and degradation) in membrane-bound carriers called vesicles. Their trafficking within the confines of the cell is regulated during the vesicle formation – where it forms, which proteins get in and where the vesicle goes. A major regulator for the initiation of vesicle formation is a small GTPase named ARF, which acts as a molecular switch, and its activator guanine-nucleotide exchange factor (GEF, or ARF-GEF). Inactive ARFs are soluble, whereas active ARFs reside on intracellular membranes, where they recruit coatomer coat proteins required for vesicle formation and cargo selection. All ARF-GEFs have a catalytic domain that on their own can mediate guanine-nucleotide exchange on ARF in a test tube. In the cell, however, ARF-GEFs form homodimers, that is a complex of two identical subunits.

Question: Why do Arabidopsis ARF-GEF proteins exist as dimers of identical subunits, each able to activate one ARF1 molecule? Is there some coordination during ARF1 activation, what is its consequence and what happens if coordinated activation fails? We focused here on the ARF-GEF GNOM.

Findings: We showed that GNOM always exists as a dimer, regardless of whether or not it is activating ARF1. One GNOM interacts with two ARF1 molecules at the membrane at the same time, as shown by blocking the exchange reaction. As consequence of coordinated activation, ARF1 proteins are inserted into the membrane next to each other, only 10 nm or less apart. Genetic inactivation of *ARF1* strongly impaired vesicle trafficking. Similarly, mutations in GNOM that reduce the coordinated activation if two ARF1 molecules by the catalytic domains of the ARF-GEF dimer also interfered with vesicle traffic. Thus, coordinsted activation of two ARF1 GTPases results in their close spacing in the vesicle-foming membrane and appears essential for membrane traffic,

Next steps: Different members of the Arabidopsis ARF-GEF family share ARF1 as their common substrate, although they regulate different trafficking pathways. In the future, we wish to analyze if dimerization of other ARF-GEFs is involved in their subcellular localization and contributes to the specification of trafficking pathways.

the hydrolysis-deficient ARF1-Q71L (Dascher and Balch, 1994; Singh et al., 2018), for their interaction with endogenous ARF1 by coimmunoprecipitation (Figure 1; for an overview of mutant proteins, see Supplemental Figure 1). We generated stable transgenic lines in the wild-type Columbia (Col-0) background that expressed ARF1, ARF1-T31N, or ARF1-Q71L in an estradiol-inducible fashion. Both ARF1-T31N and ARF1-Q71L coprecipitated endogenous ARF1, although wild-type ARF1 failed to do so (Figure 1A). These results suggested a transient and/or weak interaction between wild-type ARF1 proteins. Coimmunoprecipitation revealed that ARF1-T31N strongly interacted with the ARF-GEF GNOM but ARF1-Q71L did not (Figure 1A), revealing their qualitatively different interactions: two activation-deficient ARF1 molecules (caused by the T31N substitution) might be bridged by each ARF-GEF dimer, whereas activated ARF1 molecules (stabilized by the Q71L substitution) might interact independently of ARF-GEF. We also generated transgenic Arabidopsis lines in the Col-0 background expressing an engineered homolog of the reported dimerization-deficient ARF1-Y35A mutant (see Introduction; Beck et al., 2008, 2011). In coimmunoprecipitation experiments with seedling extracts, ARF1-Y35A-YFP associated with ARF-GEF GNOM but only weakly with endogenous ARF1 and thus behaved essentially like wild-type ARF1 (Figure 1B). Cell fractionation indicated that GNOM dimers are constitutive, since they were detected in both the S100 cytosolic fraction and the P100 membrane fraction (Figure 1C). By contrast, we detected no interaction between GNOM and ARF1 in either fraction. The P100 fraction had to be solubilized harshly for the subsequent coimmunoprecipitation experiment, which might have abolished any transient interaction of ARF1 with GNOM. We therefore attempted to stabilize the ARF1-GNOM interaction by pretreatment with (and continued exposure to) the fungal toxin brefeldin A (BFA), which causes abortive ARF1●ARF-GEF complexes by inhibiting the GDP-GTP exchange reaction (Peyroche et al., 1999; Robineau et al., 2000; Geldner et al., 2003). BFA treatment did reveal an interaction between ARF1 and GNOM in the P100 fraction but not in the S100 fraction, supporting the view that two ARF1●GDPs are bridged by each GNOM dimer present on the membrane (Figure 1D).

To assess the presumed interaction among ARF1●GTPs in a different way, we performed FRET-FLIM (fluorescence resonance energy transfer-fluorescence lifetime imaging microscopy) measurements on transgenic Arabidopsis lines coexpressing YFP- and RFP-tagged versions of the ARF1 variants under the control of the estradiol-inducible promoter. FRET-FLIM effects are known to depend on the close physical proximity of the proteins involved (Bücherl et al., 2014). If the proteins involved are <10 nm apart, the fluorescence lifetime of the donor (YFP) will be reduced by energy transfer to the acceptor (RFP). Our measurements suggested an interaction between ARF1-Q71L proteins in seedling root cells, which was prevented when combined with the Y35A mutation (Figures 1E and 1F). By contrast, the ARF1-T31N variant showed only a slight lifetime reduction in the same FRET-FLIM assay. Furthermore, this mild effect was not suppressed by the Y35A mutation (Figure 1F). In conclusion, these experiments strongly suggested the close proximity (<10 nm) of ARF1●GTP proteins on the membrane where these ARF1 molecules had been activated by ARF-GEF dimers.

To examine the biological significance of closely spaced membrane-inserted ARF1●GTP molecules, we analyzed the ability of ARF1-Y35A to rescue the secretion of α-amylase from tobacco (*Nicotiana tabacum*) protoplasts that had been blocked by the expression of the ARF1-T31N variant (Figures 2A and 2B). Increasing amounts of cotransfected wild-type ARF1 plasmid

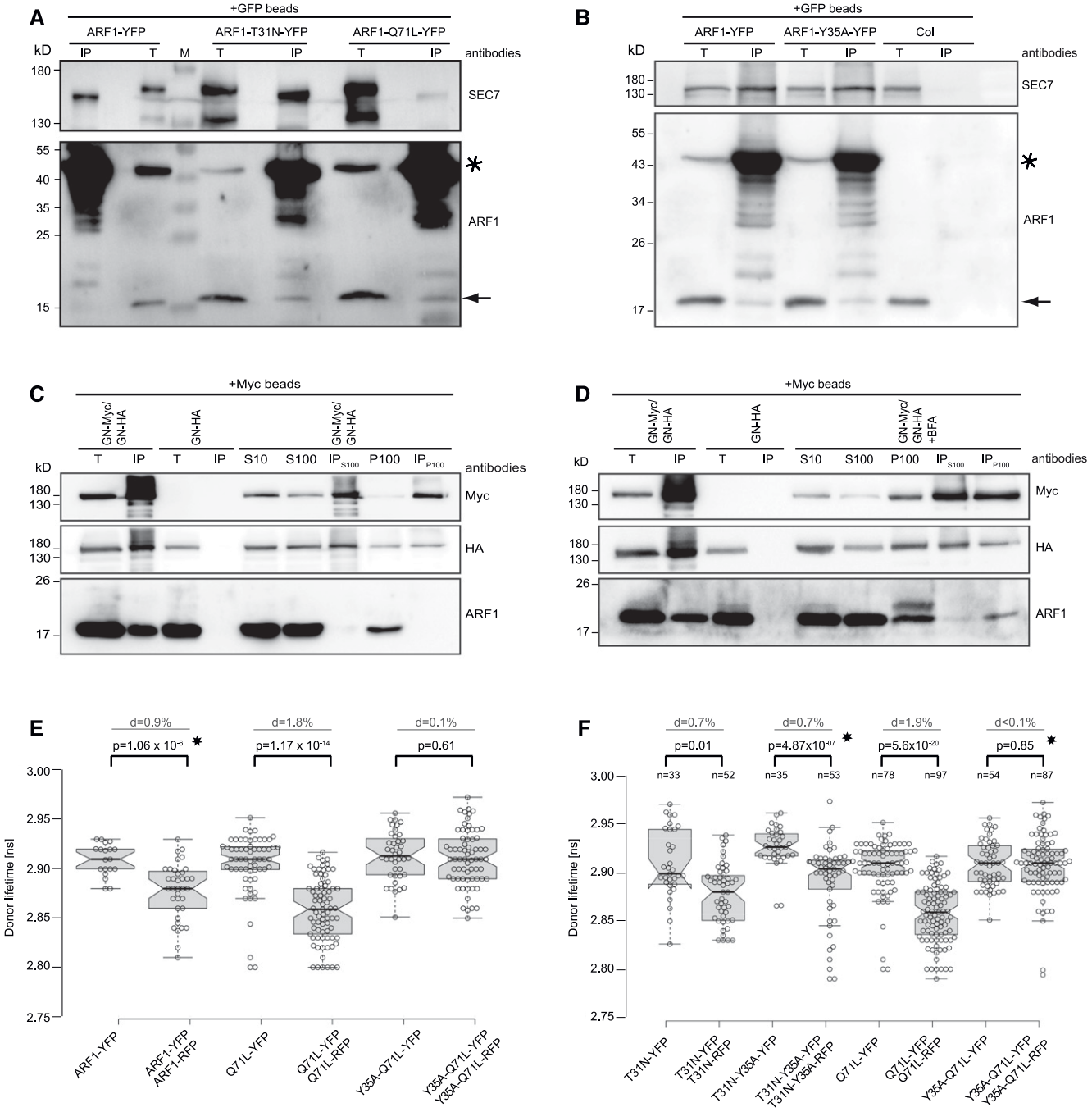

Figure 1. In Vivo Interactions between ARF-GEF and ARF1.

(A) to **(D)** Coimmunoprecipitation experiments with protein extracts from Arabidopsis seedlings treated with 20 μM estradiol for 7 h. IP, immunoprecipitate; M, molecular mass markers (sizes in kD); T, total. Antibodies are indicated on the right; ARF1-YFP fusion (asterisk) and endogenous ARF1 (arrow) were detected with anti-ARF1 antiserum.

(A) and **(B)** Interaction of YFP-tagged wild-type and mutant forms of ARF1 (T31N, Q71L, and Y35A) with endogenous ARF1 and ARF-GEF GNOM (anti-SEC7 antiserum). Col-0 was used as a negative control.

(C) and **(D)** Cell fractionation followed by coimmunoprecipitation in the absence **(C)** or presence **(D)** of 50 μM BFA. Subcellular fractionation and immunoprecipitation of GNOM-Myc from seedlings expressing double-tagged GNOM (GN-Myc and GN-HA) was performed using α-Myc-agarose beads on S10 (in the case of control immunoprecipitate), S100 (IP_{S100}), and solubilized P100 (IP_{P100}) followed by immunoblot analysis with anti-Myc, anti-HA, and anti-ARF1 antisera. A transgenic line expressing only GN-HA was used as a negative control. S10, supernatant of 10,000*g* centrifugation; S100 and P100, supernatant (cytosol) and solubilized pellet (membrane fraction) of 100,000*g* centrifugation.

DNA overcame the inhibition imposed by ARF1-T31N. By contrast, cotransfection of protoplasts with comparable amounts of ARF1-Y35A plasmid DNA largely failed to restore α-amylase secretion to the same levels as wild-type ARF1 (Figure 2A). In addition, strong expression of ARF1-Y35A interfered with α-amylase secretion on its own (Figure 2B). Thus, close proximity of ARF1 proteins inserted into the membrane appears necessary for ARF1-dependent membrane trafficking. We also analyzed the consequences of ARF1-Y35A overexpression in seedling root cells at the ultrastructural level (Figures 2C and 2D; Supplemental Figure 2). ARF1-Y35A disrupted the organization of the Golgi/trans-Golgi network, resulting in strings of interconnected membrane vesicles of variable sizes, whereas overexpression of wild-type ARF1 protein only caused a slight bending of Golgi stacks. That both the Golgi and trans-Golgi network were affected is consistent with the localization of ARF1-YFP to these subcellular compartments, as detected with gold-labeled anti-GFP antibodies (Singh et al., 2018). However, overexpression of ARF1-Y35A did not interfere with membrane recruitment of the coatomer (COPI) subunit γCOP (Figure 2E), suggesting that interaction with effectors might not be impaired. In conclusion, close proximity of ARF1●GTP proteins is essential for membrane trafficking.

Coordinated Activation of Two ARF1 Molecules by GNOM Dimers at the Membrane

How are ARF1●GTP molecules inserted close to each other into the membrane? Closely spaced insertion may require a chaperone, and an obvious candidate is the activating ARF-GEF, which itself forms dimers (Figures 1C and 1D; Ramaen et al., 2007; Anders et al., 2008). In the case of human GBF1, ARF1●GDP binding by ARF-GEF involves the C-terminal loop after helix J (loop>J) of the SEC7 domain, as demonstrated by specific mutations that interfere with ARF1 binding (Lowery et al., 2011). We introduced homologous mutations into Arabidopsis GNOM to generate GN-loop>J(3A) mutant protein (Figure 3A). To assess the biological consequences of the *GN-loop>J(3A)* mutation, we analyzed the phenotypes of plants expressing the GN-loop>J(3A) mutant protein in various *gnom* mutant backgrounds (Figures 3B to 3G). The GN-loop>J(3A) mutant protein displayed some residual activity, as it partially rescued the *gnom-sgt* deletion that spans *GNOM* and four adjacent genes on either side (Figures 3B and 3E). Interestingly, GN-loop>J(3A) mutant protein exhibited the same incomplete rescue on the strong *gnom* alleles *emb30-1* and *B4049*, which are functionally equivalent to complete loss-of-function alleles but can complement each other in the *trans*-heterozygous state (Figure 3E; Supplemental Figure 1; Busch et al., 1996; Anders et al., 2008). *gnom* mutant seedlings partially rescued by the GN-loop>J(3A) mutant protein were phenotypically similar to the weak allele $gnom^{R5}$ (Geldner et al., 2004). While $gnom^{R5}$ encodes a C-terminally truncated GNOM protein that accumulated to reduced levels compared with the wild type, the GN-loop>J(3A) mutant protein appeared to accumulate at about wild-type levels, as determined with an antibody raised against GNOM (Figures 3F and 3G). To assess the accumulation of the GN-loop>J(3A)-Myc mutant protein relative to GNOM-Myc protein, which rescues the *gnom-sgt* deletion mutant, we then probed the protein extracts with an anti-Myc antibody (Figures 3H and 3I). Although accumulating at a higher level than the rescuing GNOM-Myc protein, the GN-loop>J(3A)-Myc mutant protein failed to rescue the *gnom-sgt* deletion mutant, suggesting a primary defect in protein function rather than protein or RNA stability (Figures 3H and 3I). A more detailed phenotypic analysis of partially rescued seedlings revealed $gnom^{R5}$-like defects in cotyledon vasculature, lateral root initiation, and primary root growth, regardless of the *gnom* mutant background (Figures 4A to 4C). In the wild-type background, GN-loop>J(3A) had no noticeable phenotypic effects: primary root growth, root gravitropic responses, and BFA sensitivity were all normal (Figures 4C and 4D). Much later during development, plants bearing the *GN-loop>J(3A)* construct had twisted rosette leaves, similar to *emb30/B4049 trans*-heterozygous plants, but subsequently they grew to a normal height during flowering (Figure 5). In conclusion, the GN-loop>J(3A) mutant protein retains some residual activity but also has a fundamental defect that cannot be rescued by the complementing *gnom* alleles *emb30-1* and *B4049*.

Because the human ARF-GEF GBF1 displayed impaired ARF1 binding when carrying a J-loop mutation (Lowery et al., 2011), we tested ARF1-GNOM interactions in the context of the GN-loop>J(3A) mutant using coimmunoprecipitation assays. ARF1-YFP was coimmunoprecipitated with Myc-tagged wild-type GNOM protein but not with the Myc-tagged GN-loop>J(3A) mutant protein, using either anti-GFP or anti-Myc beads (Figures 6A and 6B). This compromised interaction between GN-loop>J(3A) and ARF1●GDP was consistent with a mutant phenotype corresponding to a low level of ARF-GEF activity for GNOM, as described above (Figures 3B to 3G and 4). The residual activity of the GN-loop>J(3A) mutant protein suggested that its strongly reduced interaction with ARF1 might be below the detection limit of the assay. We therefore attempted to stabilize the presumed interaction between mutant ARF-GEF and ARF1 by using transgenic seedlings that expressed activation-deficient ARF1-T31N-YFP in an estradiol-inducible manner, as the T31N mutation blocks the GDP-GTP exchange (Dascher and Balch, 1994). This experimental modification allowed the detection of an interaction between the GN-loop>J(3A) protein and ARF1 in the coimmunoprecipitation assay (Figure 6C). This result suggested that ARF1

Figure 1. (continued).

(E) and **(F)** FRET-FLIM analysis of wild-type and mutant ARF1-ARF1 interactions. Arabidopsis seedlings were treated with 20 μM estradiol for 4 h before FRET-FLIM analysis. Data are shown as box plots of donor lifetimes (in ns) pooled from two to three independent experiments for each sample. Medians are shown as center lines, notches indicate 95% confidence intervals, and Tukey whiskers indicate 1.5× the interquantile range. Exemplary P values (two-tailed *t* test assuming equal variances, $\alpha = 0.05$; *, two-tailed *t* test assuming unequal variances, $\alpha = 0.05$) are indicated in the graph. d, difference of median between experimental and control values shown as percentage of the control value. For raw data and statistics, see the Supplemental Data Set.

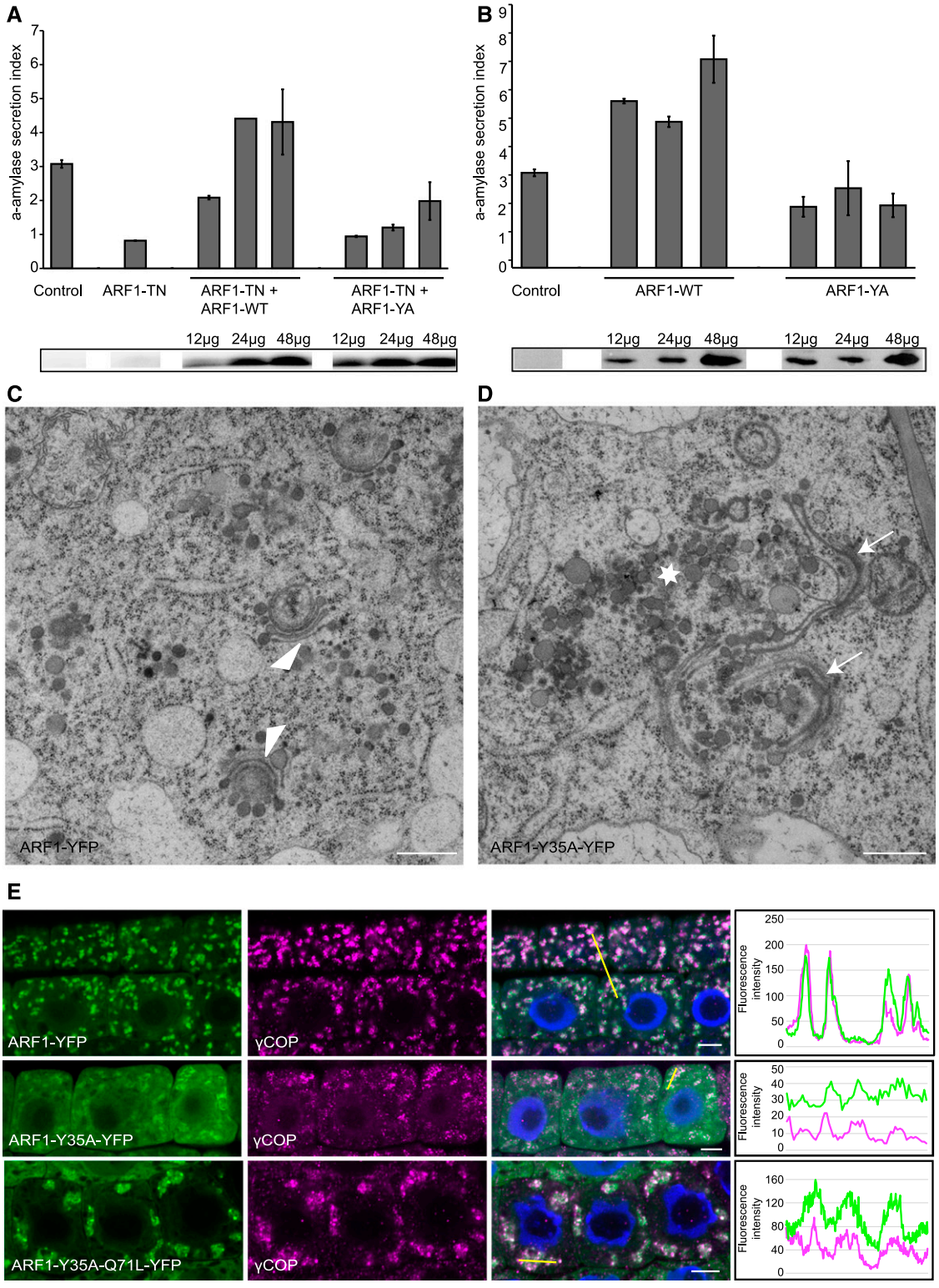

Figure 2. Biological Consequences of ARF1-Y35A Overexpression.

(A) and **(B)** Secretion of α-amylase from tobacco protoplasts inhibited by ARF1-TN (T31N) was restored by overexpression of wild-type ARF1 (ARF1-WT) but not ARF1-Y35A (ARF1-YA; **[A]**) and impaired by ARF1-YA compared with ARF1-WT **(B)**. For ARF1-WT and ARF1-YA, 12, 24, and 48 µg of plasmid DNA was used for transformation. For all ARF1-TN-containing samples, 1 µg of DNA was transformed. All samples were cotransfected with a constant amount of

binding was impaired but the GN-loop>J(3A) protein was still able to carry out the GDP-GTP exchange, consistent with the partial rescue of the *gnom-sgt* deletion.

The fungal toxin BFA inhibits the exchange reaction and therefore stabilizes abortive complexes of ARF-GEF and ARF1●GDP on endomembranes (Figure 1D; Geldner et al., 2003; Mossessova et al., 2003; Renault et al., 2003). Treating seedling roots with BFA resulted in colocalization of GNOM and ARF1 in endosomal membrane aggregates called BFA compartments (Figure 6D; Geldner et al., 2003). By contrast, colocalization of GN-loop>J(3A) with ARF1 in BFA compartments was strongly reduced, thus resembling that of the engineered BFA-resistant GNOM-M696L variant in ARF1-positive BFA compartments (Figure 6D). This result left one open question: is the membrane association of GN-loop>J(3A) reduced, or is the diminished BFA response due to impaired ARF1 binding? Cell fractionation of seedling extracts demonstrated that the GN-loop>J(3A) mutant protein partitioned between the cytosol and the membrane fraction like wild-type GNOM protein (Figures 6E and 6F). The membrane association of GNOM requires interaction between its DCB domain and the complementary fragment called ΔDCB, which does not occur in the membrane association-deficient mutant protein GNOM(B4049; Anders et al., 2008). A yeast two-hybrid assay to test for interaction between DCB and ΔDCB was positive when the ΔDCB domain carried the GN-loop>J(3A) mutation, similar to the DCB-ΔDCB interaction seen for wild-type GNOM and unlike GNOM(B4049) (Figure 7). In conclusion, several lines of evidence suggest that the GN-loop>J(3A) mutant protein exhibits normal membrane association activity and that its insensitivity to BFA is consistent with reduced ARF1 binding.

Like other ARF-GEFs, GNOM forms dimers (Figures 1C and 1D; Grebe et al., 2000; Anders et al., 2008). Coimmunoprecipitation with anti-Myc or anti-GFP beads revealed that Myc-tagged GN-loop>J(3A) mutant protein can dimerize with GNOM-GFP protein (Figure 8A). However, endogenous ARF1 was only detected in the precipitate of anti-GFP beads but not in the precipitate of anti-Myc beads, which suggested that heterodimers consisting of one wild-type GNOM and one GN-loop>J(3A) mutant molecule failed to interact with ARF1, much the same way as GN-loop>J(3A) homodimers did not detectably interact with ARF1 (Figures 8A and 8B; compare with Figures 4A to 4C). This puzzling result is however consistent with the observation that the accumulation of the GN-loop>J(3A) mutant protein failed to rescue both *emb30-1* and *B4049 gnom* alleles, as described above (Figures 3 and 4; Supplemental Figure 1; Anders et al., 2008). These results suggest that a strong interaction between ARF1 and its exchange factor requires the simultaneous binding of two ARF1●GDP molecules by the two SEC7 domains of the ARF-GEF dimer.

A Model for the Generation of Close-Proximity, Membrane-Associated ARF1 GTPases by Coordinated Activation by ARF-GEF Dimers

We propose the following model to explain how membrane-associated ARF1 GTPases are brought in close proximity to form membrane vesicles (Figure 9). Cytosolic GDP-bound ARF1 molecules exist as monomers. They interact with membrane-associated ARF-GEF dimers, with the loop after helix J of the SEC7 domain playing a critical role for ARF1 binding. Productive complex formation requires cooperativity (i.e., simultaneous interaction of two ARF1●GDP molecules with the two SEC7 domains of an ARF-GEF dimer). As a consequence, two adjacent ARF1 molecules undergo a conformational change, resulting in GDP-GTP exchange and the insertion of the myristoylated N terminus of the two ARF1●GTP molecules into the membrane, less than 10 nm apart, since they were bridged by the same ARF-GEF dimer (Figure 9A). One might speculate that wild-type ARF1●GTP molecules might only form weakly interacting homodimers that may not be readily detected by typical protein extraction procedures, especially since there is a large excess of cytosolic ARF1●GDP (Figure 1C). This possibility is supported in vitro by the rescue of the vesicle scission defect normally caused by the ARF1-Y35A variant by forced chemical cross-linking (Beck et al., 2011). Alternatively, the close proximity of coordinately activated ARF1 GTPases might be stabilized by spatial constraints of interacting coat protein complexes. Regardless of whether or not ARF1●GTP proteins form dimers, the close proximity of ARF1●GTP proteins is biologically relevant: reducing the efficiency of the coordinated activation by ARF-GEF dimers of wild-type GNOM and mutant GN-loop>J(3A) interfered with membrane trafficking, as did altering the proximity of ARF1 proteins due to the Y35A substitution (Figure 9B). Whether the primary defect entails abnormal coat lattice formation and/or impaired scission of membrane vesicles remains to be determined, although the latter agrees with previous in vitro studies (Beck et al., 2011; Arakel and Schwappach, 2018). In the normal course of events, following vesicle scission, GTPase activation protein (GAP)-assisted hydrolysis of GTP would alter the conformation of ARF1, thereby disrupting the close proximity and releasing monomeric ARF1●GDP back into the cytosol (Figure 9A). Considering the conservation of the overall domain organization of large ARF-GEFs (Casanova, 2007; Bui et al., 2009), it is highly likely that

Figure 2. (continued).

α-amylase reporter plasmid. Error bars depict SD of two independent experiments. Bottom panels show antibody detection of GFP linked to ARF1 expression. Control, α-amylase reporter plasmid only.

(C) and **(D)** Electron microscopy analysis of epidermal cells at the upper end of the seedling root meristem expressing ARF1-YFP **(C)** or ARF1-Y35A-YFP **(D)** in response to 10 μM estradiol for 4 h. Arrowheads, bent Golgi stacks; asterisk, cluster of interconnected membrane vesicles; arrows, Golgi remnants. See also Supplemental Figure 2. Bars = 500 nm.

(E) Immunostaining of the COPI subunit γCOP in seedling root cells expressing ARF1-YFP, ARF1-Y35A-YFP, or ARF1-Y35A-Q71L-YFP in response to 20 μM estradiol for 4 h. ARF1 variant (green), γCOP (magenta), and merged images with 4′,6-diamidino-2-phenylindole-stained nuclei (blue) are shown. Colocalization of ARF1 and γCOP in regions of interest (yellow lines) are shown as line intensity profiles. Bars = 5 μm.

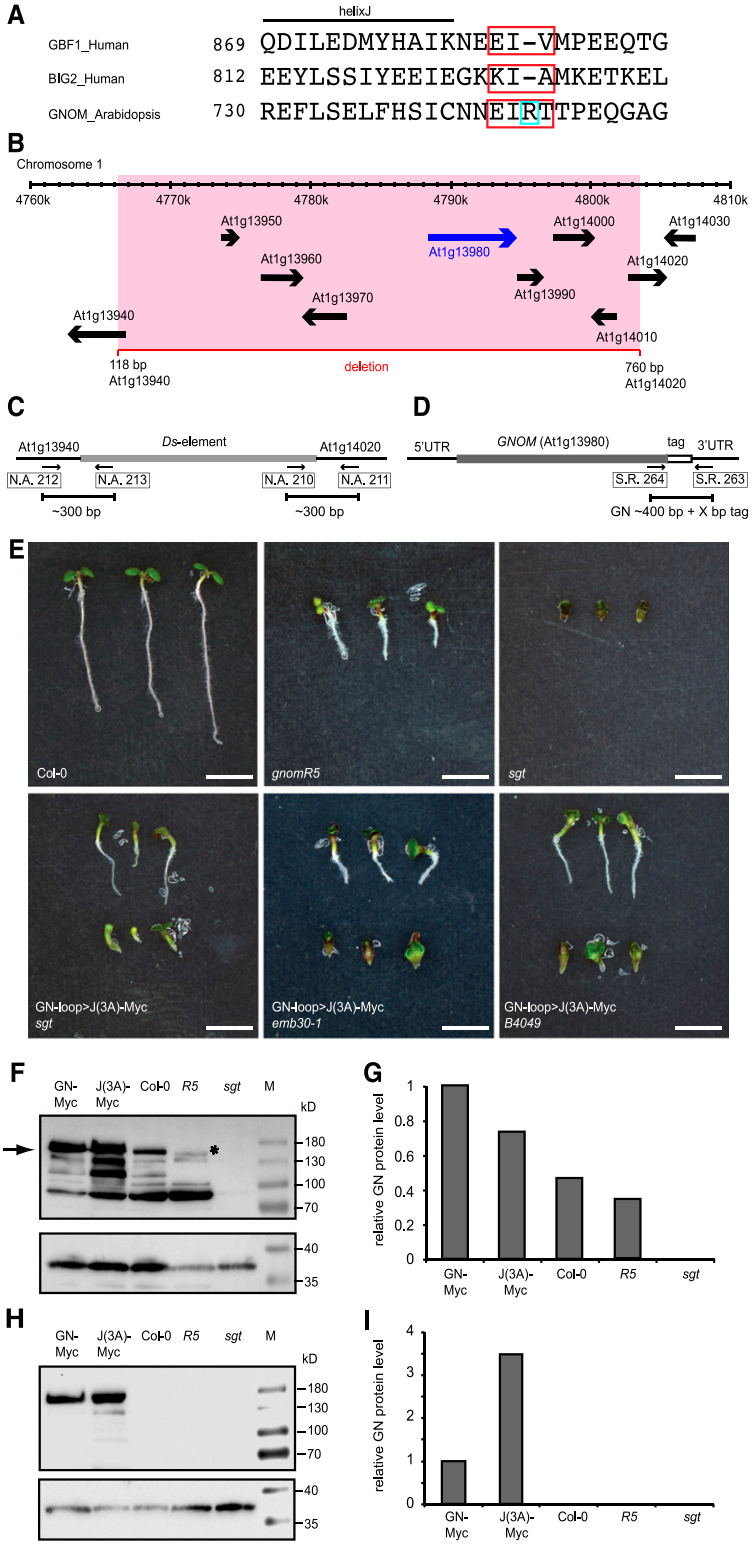

Figure 3. Rescue Activity of GN-loop>J(3A)-Myc in *gnom-sgt* Deletion and Other *gnom* Mutants.

(A) Ala substitution sites (red boxes) in the loop after helix J (loop>J) of the SEC7 domain of human GBF1 (Lowery et al., 2011), human BIG2 (Lowery et al., 2011), and Arabidopsis GNOM. In GN-loop>J(3A) mutant protein, amino acid residues 744 to 747 (EIRT) are replaced by AARA.

cooperative ARF1 binding by ARF-GEF dimers as a mechanism of forming active ARF1 proteins arranged in close proximity on the donor membrane applies to eukaryotes in general.

METHODS

Plant Material, Genotyping, and Growth Conditions

Arabidopsis (*Arabidopsis thaliana*) plants were grown in constant light (Osram L18W/840 cool-white lamps; 200 μmol m^{-2} s^{-1}) at 23°C and 40% humidity in growth chambers on soil or agar plates. Previously published lines that were used in this study are as follows: the strong *gnom* mutant alleles *B4049* and *emb30-1*, the *trans*-complementing *B4049/emb30-1* heterozygote (Busch et al., 1996), and the weak allele *gnom*^{R5} (Geldner et al., 2004), as well as transgenic lines expressing GNOM-Myc, BFA-resistant GNOM-M696L-Myc, or GNOM-GFP from the *GNOM* promoter (Geldner et al., 2003), ARF1-YFP from the *RPS5A* promoter, and ARF1-T31N-YFP and ARF1-Q71L-YFP from an estradiol-inducible promoter system (Singh et al., 2018).

There are six Arabidopsis genes encoding ARF1 proteins with at least 98% identity (Singh et al., 2018). The ARF1 protein under study here and used for generating the antiserum was ARF1A1C (gene identifier At2g47170). For simplicity, we have designated ARF1A1C as ARF1 in the text. It should be noted, however, that the antiserum also detects the other five proteins ARFA1B to ARFA1F (Singh et al., 2018).

For the *gnom-sgt* mutant, the Ds-induced *sgt* allele was generated during an Ac-Ds mutagenesis experiment and isolated for its *gnom*-like mutant phenotype (insertion line SGT2467; Kumaran et al., 1999). The deletion on chromosome 1 eliminates nine genes from At1g13940 (5′ end of *Ds*) to At1g14020 (3′ end of *Ds*), including *GNOM* (At1g13980; Figure 3B).

For genotyping, we used the following primers (listed in Figure 3 and Supplemental Table 1). Primers N.A.212 + N.A.213 and N.A.210 + N.A.211 generate a PCR product of 270 bp in the *gnom-sgt* mutant background. Primers S.R.264 + S.R.263 were used to confirm the presence of the Myc-tagged *GNOM* transgene (expected sizes, 373 bp for wild-type *GNOM* and 496 bp for the Myc-tagged *GNOM*). This primer pair will not amplify *gnom-sgt*. Primers M.E.N.64 and M.E.N.66 were used to detect the presence of the *B4049* mutation in *B4049*/+ heterozygous seedlings; they generate a PCR product of 535 bp only for the *B4049* allele, whereas the wild-type allele will give no product. The complementary primer pair M.E.N.65 and M.E.N.66 will however amplify a PCR product specifically for the wild-type allele and not the B4049 allele (expected size, 535 bp).

Genotyping for the *emb30-1* allele was performed in two steps. First, a *GNOM* PCR product of 2496 bp that includes the *emb30-1* mutation was amplified with primers S.R.36 + S.R.87. This PCR product was then used as a template for a second PCR reaction with primers S.R.36 + S.R.37 to yield a 357-bp product (for both wild-type and *emb30-1* alleles), which was then digested with the restriction enzyme *Hin*fI to distinguish the *emb30-1* mutant allele from the *GNOM* wild-type allele in the segregating *emb30*/+ population (expected restriction patterns: wild-type allele, 193, 65, 47, 32, and 20 bp; *emb30-1* allele, 193, 97, 47, and 20 bp).

Binary Vector Constructs, Generation of Transgenic Plants, and Crosses

To generate the loop>J(3A) mutation, we changed amino acid residues 744, 745, and 747 [EI(R)T] to Ala (AARA) by site-directed mutagenesis. Mutagenesis PCR was performed on the genomic fragment GNXbaI^{wt}-Myc (Geldner et al., 2003) in pBluescript, using the primers Loop>J(3A) sense and Loop>J(3A) rev.

The *GNpro*:*GN-loop>J(3A)XbaI-Myc* fragment was cloned at the *Xba*I restriction site into the pGreenII(Bar) binary vector, introduced into *Agrobacterium tumefaciens* strain GV3101 (carrying resistance genes for tetracycline, rifampicin, and gentamicin), and transformed into Arabidopsis accession Col-0. Primary transformants were selected on soil on the basis of resistance to glufosinate spraying. Four different transgenic lines showed good expression, and two were chosen for further analysis.

GN-loop>J(3A)-Myc #5 was crossed into the *sgt*, *B4049*, and *emb30-1* backgrounds and analyzed for complementation. For coimmunoprecipitation analysis, *GN-loop>J(3A)-Myc* was crossed with *RPS5Apro*:*ARF1-YFP* or *ESTpro*:*ARF1-T31N-YFP*, and *GN-loop>J(3A)-Myc* (*sgt* heterozygous background) was crossed with *GNOM-GFP*.

To generate an estradiol-inducible variant of wild-type ARF1-YFP, we used a modified β-estradiol-inducible pMDC7 vector in which the *UBIQUITIN10* promoter replaced the original 35S promoter to drive expression of the XVE chimeric transcription factor (Singh et al., 2018). We performed site-directed mutagenesis on pENTRY-ARF1-T31N-YFP (Singh et al., 2018), using the ARF1 primer combination ARFA1C-WT-MUT-S and ARFA1C-WT-MUT-AS to generate pENTRY-ARF1-YFP, which was subsequently introduced into the *UBQ10pro*:*XVE;LexApro*:*(Gene Of Interest)* vector.

The Y35A mutation was introduced into pENTRY-ARF1-YFP, pENTRY-ARF1-TN-YFP, and pENTRY-ARF1-QL-YFP by site-directed mutagenesis using the ARF1 primers ARFA1C-Y35A-MUT-S and ARFA1C-Y35A-MUT-AS.

Figure 3. (continued).

(B) Diagram of a 50-kb genomic segment of chromosome 1 displaying *GNOM* and adjacent genes (arrows run 5′ to 3′ along each gene). The *GNOM* gene is highlighted in blue. The straddling 37-kb deletion (named *gnom-sgt*) encompassing *GNOM* and eight flanking genes is indicated by a red line (Kumaran et al., 1999). End points of the deletion are indicated by bp numbers of the first and last genes.
(C) and **(D)** Primer combinations for genotyping seedlings to detect the *gnom-sgt* deletion **(C)** or the endogenous *GNOM* gene and a *GNOM* transgene encoding a C-terminally tagged protein **(D)**. The lines below the three primer combinations indicate the approximate sizes of the PCR products in bp.
(E) Wild-type seedlings (Col-0), *gnom-sgt* seedlings (*sgt*), and *gnom-sgt* seedlings bearing the *GN-loop>J(3A)-Myc* transgene. The weak *gnom*^{R5} allele is shown for comparison. Note the partial rescue of exchange-deficient *gnom* seedlings (*emb30-1*) or membrane association-deficient *gnom* seedlings (*B4049*) by the *GN-loop>J(3A)-Myc* transgene. Bars = 2.5 mm.
(F) and **(G)** GNOM protein levels in wild type (Col-0), *gnom*^{R5}, *gnom-sgt* deletion (*sgt*), and *GNOM* transgenic lines bearing *GNOM-myc* (GN-Myc) and *GN-loop>J(3A)* [J(3A)-Myc; in the Col-0 background] detected by anti-SEC7 domain antiserum. Loading control (lower panel) consisted of unstripped membrane reprobed with anti-SYP132 (SYNTAXIN OF PLANTS132) antiserum. **(F)** shows immunoblot analysis. M, molecular mass markers. The arrow indicates a GNOM band at 165 kD; the asterisk indicates a truncated GNOM protein in *gnom*^{R5} at 155 kD. **(G)** shows normalized protein levels of the immunoblot shown in **(F)**. GNOM from *GN-myc* was set to 1.
(H) and **(I)** Myc-tagged GNOM protein levels in *GNOM-Myc* and *GN-loop>J(3A)* [J(3A)-Myc] transgenic seedlings (in the Col-0 background) detected with anti-Myc antibody. Loading control (lower panel) consisted of unstripped membrane reprobed with anti-SYP132 antiserum. **(H)** shows immunoblot analysis. M, molecular mass markers. **(I)** shows normalized protein levels of the immunoblot shown in **(H)**. GNOM from *GN-myc* was set to 1.

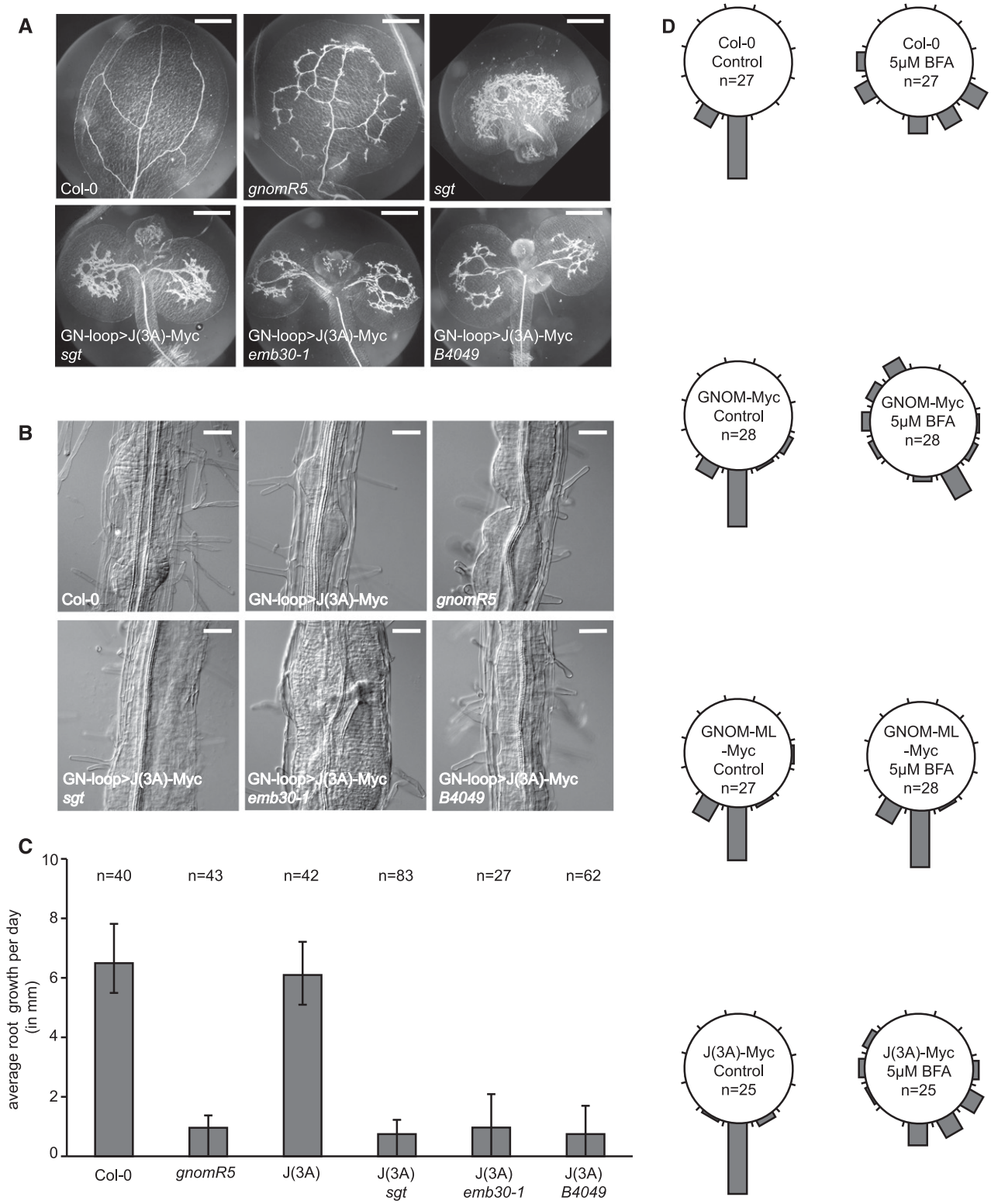

Figure 4. Seedling Phenotypes of *gnom* Mutants Bearing the *GN-loop>J(3A)-Myc* Transgene.

(A) Vascular tissue differentiation in cotyledon. Bars = 500 μm.
(B) Lateral root initiation. Bars = 50 μm.

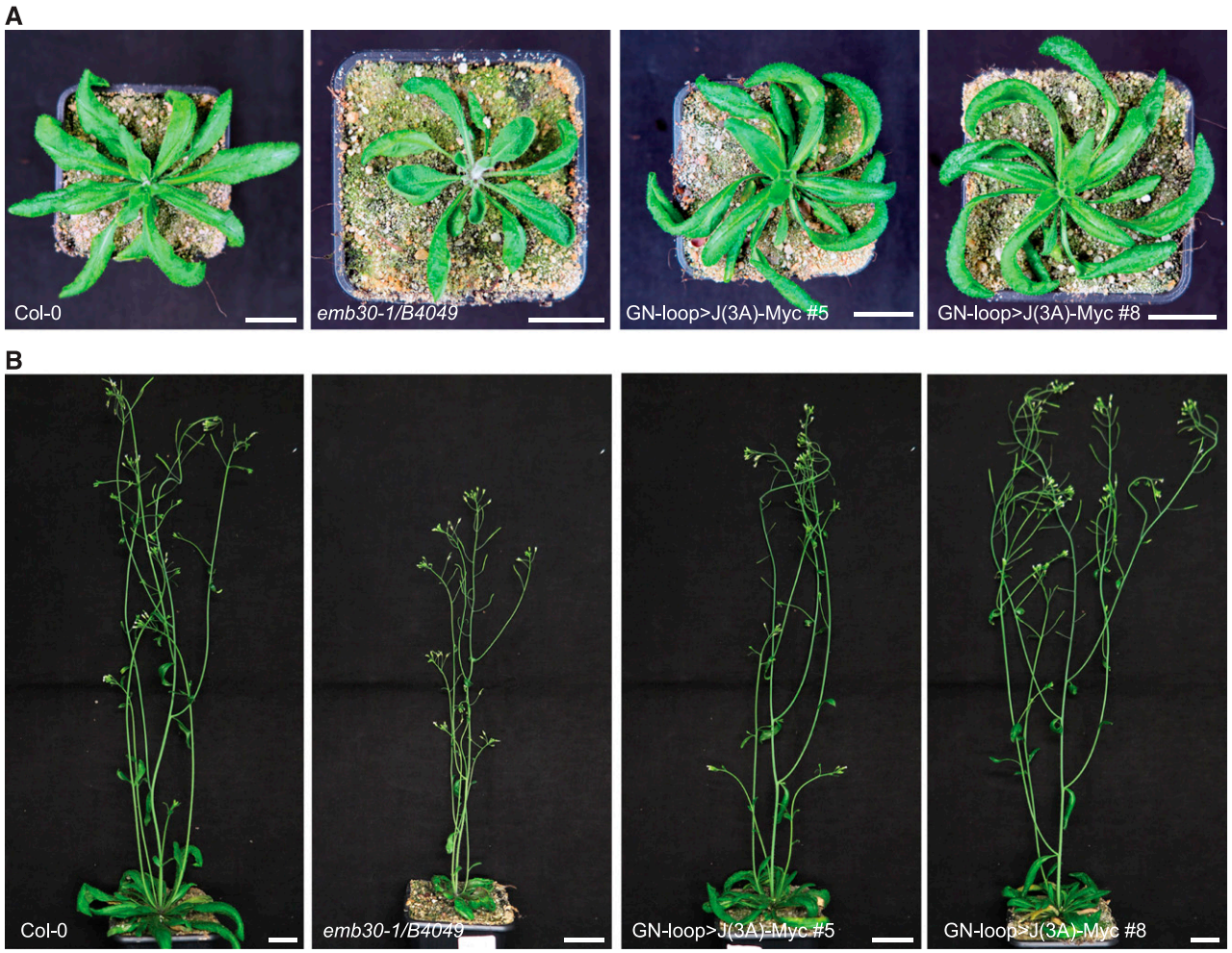

Figure 5. Developmental Phenotypes of Wild-Type Plants Expressing GN-loop>J(3A)-Myc.

(A) Rosette stage. Col-0, the wild type. Note the slightly twisted rosettes of *trans*-heterozygous plants bearing the nearly fully *trans*-complementing *gnom* alleles *emb30-1* and *B4049* and of the *GN-loop>J(3A)-Myc* transgene in Col-0 (two transgenic lines #5 and #8).
(B) Plants after the onset of flowering (same genotypes as in **[A]**). Note the nearly normal stature of *GN-loop>J(3A)-Myc* transgenic plants.
Bars = 2 cm.

To generate RFP-tagged ARF1 variants, the RFP coding sequence (with an added 5′ *Avr*II restriction site) was PCR-amplified and cloned into pDONR221 (Invitrogen), generating a pENTRY clone. The RFP gene and part of the kanamycin resistance gene from the pENTRY clone were then introduced as *Avr*II-*Ssp*I restriction fragments into the YFP-tagged ARF1 pENTRY clones mentioned above, thereby replacing the YFP tag. The different ARF1 fragments were then introduced into a modified β-estradiol-inducible pMDC7 vector by Gateway LR reaction (Singh et al., 2018).

All reagents, mutants, and transgenic lines used in this study are listed in Supplemental Table 2.

Cloning of Constructs for Transient Expression in Protoplasts

The coding sequences for ARF1, ARF1-T31N, and ARF1-Y35A were PCR-amplified from pENTRY clones mentioned above by using primers NheI-ARFA1C-S and BamHI-Stop-ARFA1C-AS. PCR-amplified ARF1

Figure 4. (continued).

(C) Primary root length (in mm). Data are shown as means ± SD. n = number of seedlings analyzed. J(3A), GN-loop>J(3A) in the wild-type background or in the different *gnom* mutant genotypes indicated (*sgt*, *emb30-1*, and *B4049*).
(D) Root gravitropism in seedlings treated with 5 μM BFA and untreated control seedlings.
GN-loop>J(3A)-myc [J(3A)] in the wild-type background behaves like Col-0 or GN-myc. Col-0, the wild type; $gnom^{R5}$, weak *gnom* allele; J(3A), GN-loop>J(3A) in the wild-type background; *sgt*, *gnom-sgt* deletion; *emb30-1*, catalytically defective $GNOM^{emb30}$; *B4049*, membrane-association-defective $GNOM^{B4049}$; *GNOM-Myc*, *GNOM-Myc* transgene; *GNOM-ML-Myc*, engineered BFA-resistant GNOM-M696L; *J(3A)-Myc*, *GN-loop>J(3A)-Myc* transgene.

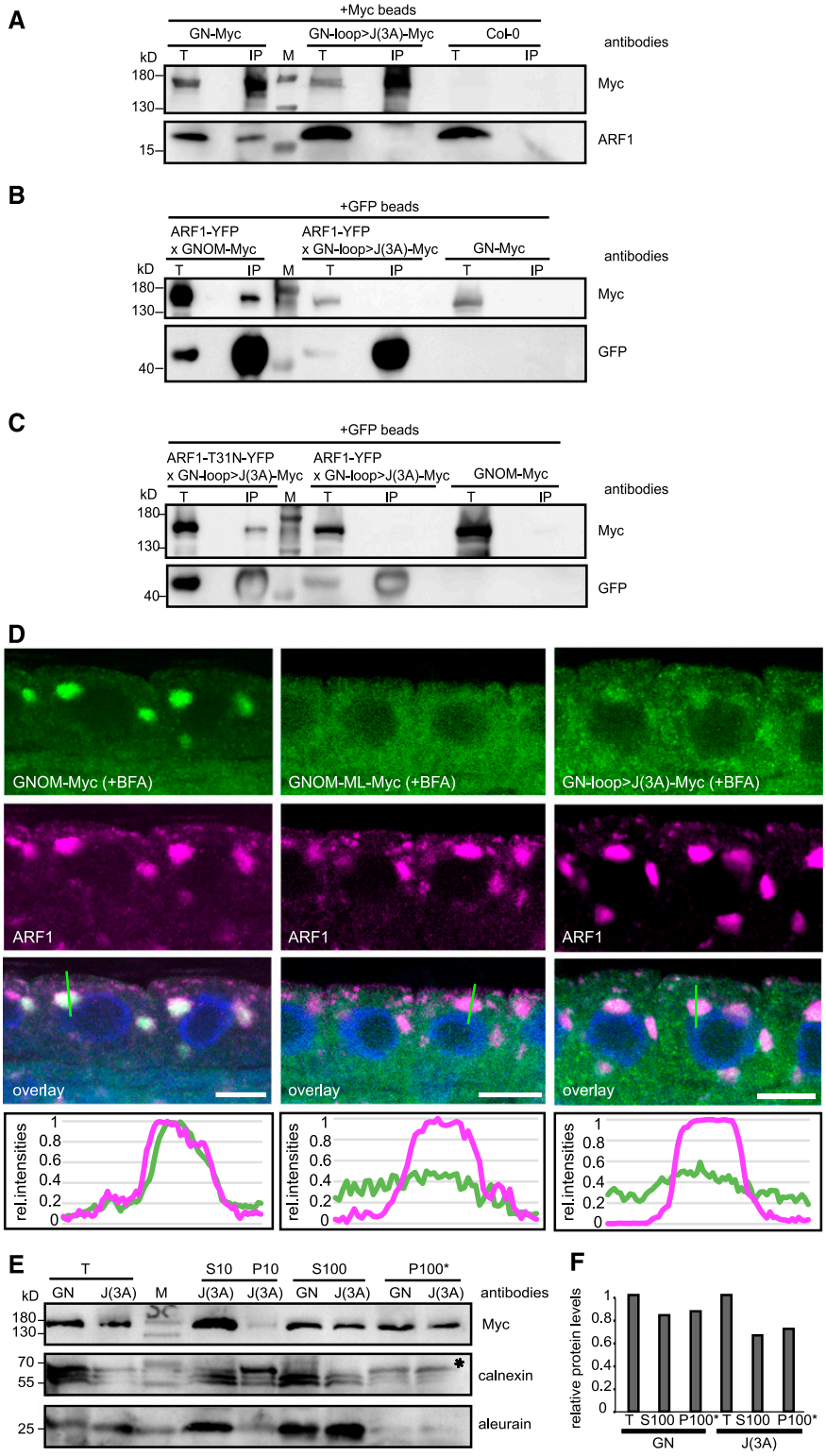

Figure 6. ARF-GEF GN-loop>J(3A) Mutant Protein: Interaction with ARF1, Subcellular Localization, and Membrane Association.

(A) to **(C)** Coimmunoprecipitation from Arabidopsis seedling extracts. No detectable interaction of endogenous ARF1 **(A)** or YFP-tagged ARF1 **(B)** with GN-loop>J(3A)-Myc compared with the GNOM-Myc wild-type control was seen following immunoprecipitation with anti-Myc beads **(A)** or anti-GFP beads **(B)**.

fragments were introduced into pFK059 (Singh et al., 2018) at the *Nhe*I and *Bam*HI restriction sites.

Physiological Tests

For primary root growth assays, we transferred 50 5-d-old seedlings to agar plates containing half-strength Murashige and Skoog (MS) agar medium with 1% (w/v) Suc and 10 μM BFA for 24 h. We analyzed seedling root growth using ImageJ software. We measured the gravitropic response of 50 5-d-old seedlings by ImageJ software after transferring seedlings to 10 μM BFA plates and rotating them by 135° for 24 h. We scored lateral root primordia formation after transferring 7-d-old seedlings for 3 d on 20 μM naphthylacetic acid (NAA)-containing half-strength MS medium with 1% (w/v) Suc agar plates and clearing the roots (Geldner et al., 2004). To examine the vasculature of 7- to 10-d-old cotyledons, we agitated seedlings for several hours in a 3:1 (v/v) ethanol:acetic acid solution at room temperature (Geldner et al., 2004). Light microscopy images were taken with an Axiophot microscope (Zeiss) and Axiocam and AxioVision_4 software (Zeiss). Image size, brightness, and contrast were adjusted in Photoshop CS3 software (Adobe).

Yeast Two-Hybrid Interaction Assays

Assay and constructs of GNOM-DCB (amino acids 1 to 246), GNOM-ΔDCB (amino acids 232 to 1451), and GNOM-ΔDCB(B4049) (amino acids 232 to 1451; G579R) were as described (Grebe et al., 2000; Anders et al., 2008). GNOM-ΔDCB(J(3A)) was generated by site-directed mutagenesis using primers mentioned above.

Quantitative Transport Assays

Tobacco (*Nicotiana tabacum*) protoplasts were prepared and transfected by electroporation as previously described (Künzl et al., 2016). Approximately 2.5×10^6 protoplasts were used for transformation per sample. The protoplast samples were transfected with a constant amount of reporter plasmid DNA (10 to 20 μg, depending on the experiment) coding for α-amylase (Bubeck et al., 2008), in addition to the amounts of ARF1 effector plasmids indicated in Figures 2A and 2B. Harvesting and analysis of medium and cell samples as well as calculation of the secretion index were performed as described (Bubeck et al., 2008). ARF1 protein accumulation levels were confirmed indirectly by the detection of GFP. Both *ARF1* and *GFP* coding sequences are placed under the control of the bidirectional *mas* promoter (consisting of a *mas1′* part and a *mas2′* part) on the same plasmid, with *mas1′* directing *GFP* expression and *mas2′* directing *ARF1* expression in a ratio of 1:10.

Whole-Mount Immunofluorescence Staining

Four- to 6-d-old seedlings were incubated on 24-well cell culture plates for 1 h in 50 μM BFA (Invitrogen, Thermo Fisher Scientific) containing liquid growth medium (half-strength MS medium and 1% [w/v] Suc, pH 5.8) at 23°C and then fixed for 1 h in 4% (w/v) formaldehyde in microtubule-stabilizing buffer at room temperature. Whole-mount immunofluorescence staining was performed manually as described (Lauber et al., 1997) or with an InsituPro machine (Intavis; Müller et al., 1998). All antibodies were diluted in 1× PBS. The following antisera were used for immunofluorescence staining: mouse anti-c-Myc mAb 9E10 (Santa Cruz Biotechnology) diluted 1:600; rabbit anti-ARF1 (Agrisera) diluted 1:1000; rabbit anti-At-γCOP (Agrisera) diluted 1:1000; anti-mouse Alexa488 (Invitrogen) and anti-rabbit CY3 (Dianova)-conjugated secondary antibodies diluted 1:600. Nuclei were stained with 4′,6-diamidino-2-phenylindole (1:600 dilution).

Confocal Microscopy and Processing of Images

Fluorescence images were acquired on a Leica confocal laser scanning microscope (TCS-SP2 or SP8) using a 63× water-immersion objective and Leica software. We also used a Zeiss confocal laser scanning microscope (LSM880) in Airy Scan mode with Zeiss software. Overlays and contrast/brightness adjustments of images were performed in Adobe Photoshop CS3 software. Intensity line profiling was performed with the Leica or Zeiss software.

FRET-FLIM Analysis

Four- to 5-d-old seedlings were incubated for 4 to 6 h in liquid growth medium (half-strength MS medium with 1% [w/v] Suc) containing 20 μM estradiol. FRET-FLIM measurements were performed on a Leica TCS-SP8 confocal microscope upgraded with the rapidFLIM system from Picoquant (TimeHarp 260 time-correlated single-photon counting module). YFP was excited with a pulsed 470-nm diode laser (LDHPC470B) with a 40-MHz pulse frequency. Emission was recorded at 495 to 550 nm by a HyD SMD detector until reaching a count of 1000 photons per pixel. We analyzed the resulting data using the SymPhoTime software. An n-exponential reconvolution with a monoexponential decay function was used to fit the time-correlated single-photon counting histograms against a measured instrumental response function (Fäßler and Pimpl, 2017; Mehlhorn et al., 2018). Box plots of measured fluorescence lifetimes were generated using the web tool tyerslab (http://boxplot.tyerslab.com; Spitzer et al., 2014). Statistical significance was calculated using a two-sample Student's *t* test. Measurements were taken from at least five different seedlings in epidermal cells near the differentiation zone of the root.

Electron Microscopy Analysis

Four- to 5-d-old ARF1-YFP and ARF1-Y35A-YFP seedlings were incubated in liquid growth medium (half-strength MS medium with 1% [w/v] Suc) containing 10 μM estradiol for 4 h. For ultrastructural analysis, 1- to 1.5-mm-long seedling root tips were high-pressure frozen, freeze-substituted in acetone containing 2.5% (w/v) OsO_4, and embedded in epoxy resin. Ultrathin sections were stained with uranyl acetate and lead citrate and viewed with a Jeol JEM-1400plus transmission electron

---

Figure 6. (continued).

In **(C)**, activation-deficient ARF1-T31N-YFP yielded coimmunoprecipitation signal of GN-loop>J(3A)-Myc following immunoprecipitation with anti-GFP beads. Col-0, the wild-type control; IP, immunoprecipitate; M, molecular weight markers; T, total extract.

(D) Immunostaining of BFA-treated seedling roots. GNOM colocalized with ARF1 whereas GN-loop>J(3A) essentially behaved like engineered BFA-resistant GNOM-M696L, not accumulating on the ARF1-positive endomembrane. Line scans are indicated with green lines.

(E) and **(F)** Cell fractionation reveals comparable partitioning between cytosol and membrane of the Myc-tagged GNOM wild type (GN) and Myc-tagged GN-loop>J(3A) mutant protein [J(3A)]. **(E)** shows immunoblots with antisera indicated on the right (controls: calnexin [asterisk] = membrane protein [Huang et al., 1993]; aleurain = soluble protein [Holwerda et al., 1990]). M, molecular mass markers. **(F)** shows the quantitation of anti-Myc signal intensities in the immunoblot shown in **(E)**. Total extracts were set to 1. T, total extract; S10 and P10, supernatant and pellet of 10,000*g* centrifugation; S100 and P100*, supernatant and washed pellet of 100,000*g* centrifugation.

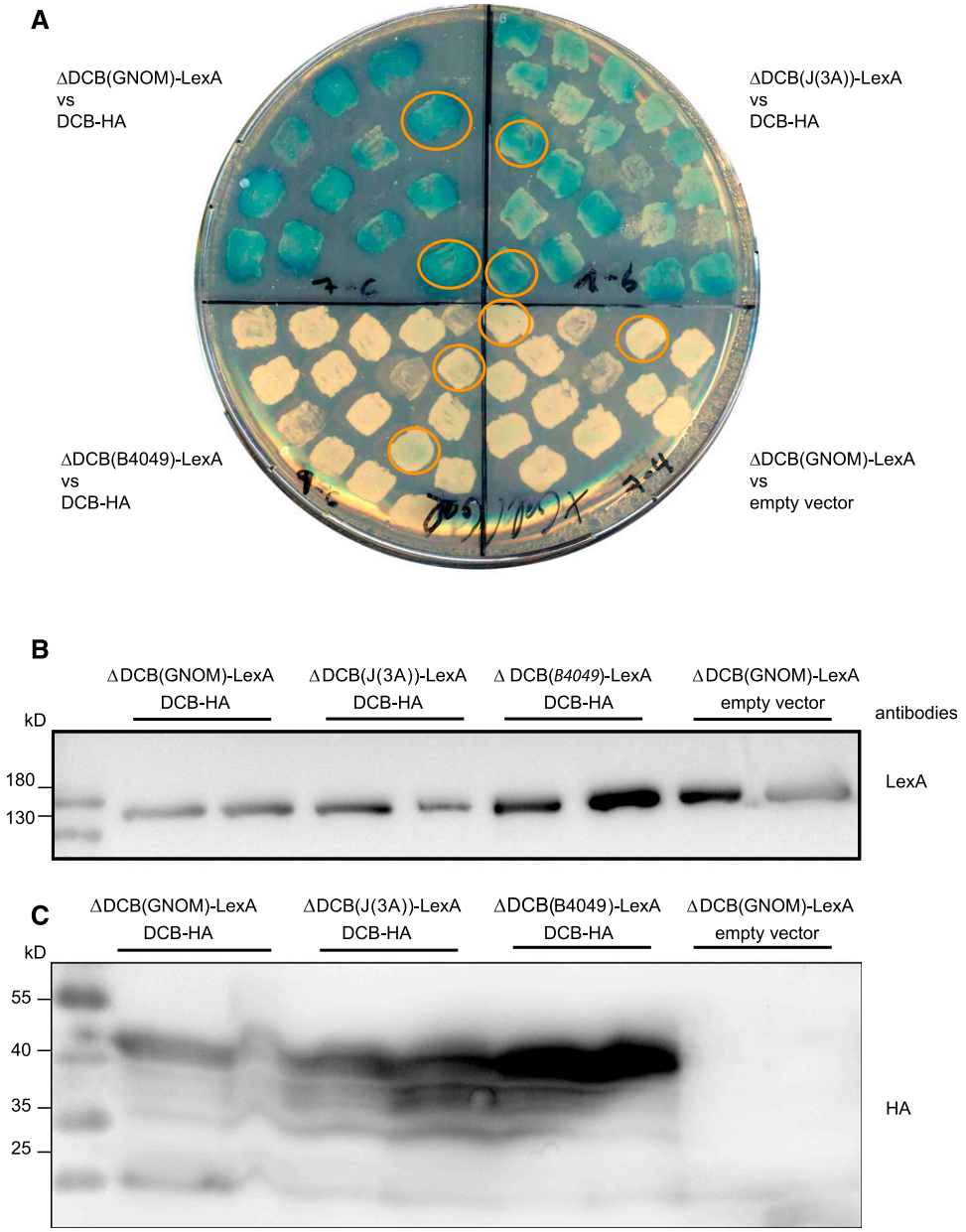

Figure 7. Y2H Assay for DCB-ΔDCB Interaction of GN-loop>J(3A).

(A) β-Galactosidase activity staining. Unlike *gnom-B4049* (negative control; lower left), GN-loop>J(3A) [J(3A)] displayed DCB-ΔDCB interaction (upper right). Upper left, the GNOM wild type (positive control); lower right, empty vector control. See also Grebe et al. (2000) and Anders et al. (2008).
(B) and **(C)** Protein levels derived from the constructs used for the interaction assay (protein extracts from circled colonies in **[B]** detected by immunoblot analysis with specific antisera indicated on the right): **(B)** LexA (DNA binding domain) fused to ΔDCB domains of GNOM wild-type (GNOM) and mutant GN-loop>J(3A) [J(3A)] and GNOM-B4049 (B4049) proteins; **(C)** HA-tagged transactivation domain fused with the DCB domain of GNOM (DCB-HA).

microscope at 120 kV accelerating voltage. For more information, see Singh et al. (2018).

Subcellular Fractionation

Two grams of plant material was ground in liquid nitrogen and suspended 1:1 in extraction buffer (50 mM Tris, pH 7.5, 150 mM NaCl, 1 mM EDTA, and 1 mM PMSF) supplemented with protease inhibitors (cOmplete EDTA-free; Roche). Of the total cell lysates, 100 μL was taken as total fraction (T). Then cell lysates were cleared by centrifugation at 10,000*g* for 10 min at 4°C and 100 μL of supernatant (S10) was saved for further analysis. The pellet was dissolved in 1 mL of extraction buffer and 100 μL was frozen (P10). After a 100,000*g* centrifugation at 4°C for 1 h, 100 μL of supernatant (S100) was stored and the pellet was dissolved in 200 μL of extraction buffer, of which

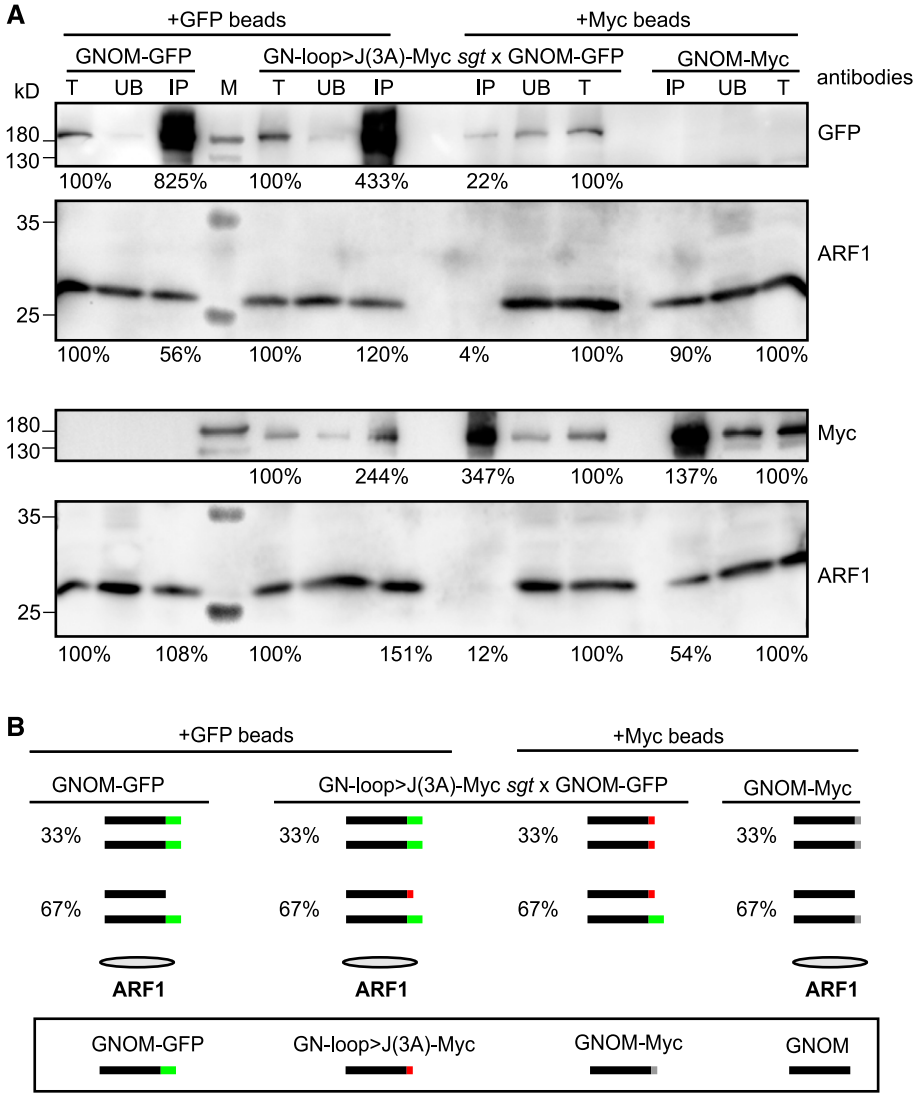

Figure 8. ARF1 Binding by ARF-GEF Dimers.

(A) Coimmunoprecipitation of GNOM-GFP and GN-loop>J(3A)-Myc from seedling extracts with either anti-GFP or anti-Myc beads reveals the interaction of GFP-tagged GNOM wild-type with GN-loop>J(3A)-Myc mutant protein and the lack of ARF1 binding by the GNOM heterodimer. Precipitates were probed with anti-GFP, anti-ARF1, and anti-Myc antisera. Percentages indicate the amount of protein bound to beads relative to total input. IP, immunoprecipitate; M, molecular mass markers; T, total extract; UB, unbound..

(B) Diagram of expected coimmunoprecipitation results showing precipitated GNOM dimers and ARF1. Tags are as follows: green = GNOM-GFP (wild type); red = GN-loop>J(3A)-Myc (mutant); gray =GNOM-Myc (wild type); no tag = endogenous GNOM. Percentages indicate the relative amount of the different GNOM homomeric and heteromeric proteins bound to beads.

100 μL was stored (P100*). A total of 25 μL of 5× Laemmli buffer was added to 100-μL samples.

Subcellular fractionation for coimmunoprecipitation was performed as above with a few modifications. After grinding, powdered plant material was suspended in 2× volume of extraction buffer and centrifuged at 10,000*g* for 15 min at 4°C. The supernatant (S10) was subjected to one 100,000*g* centrifugation at 4°C for 1 h. The supernatant (S100) was supplemented with Triton X-100 to a final concentration of 1% (v/v) and used for coimmunoprecipitation studies. The pellet (P100) was dissolved by sonication in extraction buffer containing 1% (v/v) Triton X-100 and used for coimmunoprecipitation.

Coimmunoprecipitation Analysis

The immunoprecipitation protocol was modified from Singh et al. (2014). Three to 5 g of 8- to 10-d-old Arabidopsis seedlings was homogenized 1:1 in lysis buffer (50 mM Tris, pH 7.5, 150 mM NaCl, and 1 mM EDTA) supplemented with protease inhibitors (cOmplete EDTA-free; Roche) and containing 1% (v/v) Triton X-100. Seedlings bearing estradiol-inducible ARF1-YFP, ARF1-Y35A-YFP, ARF1-T31N-YFP, or ARF1-Q71L-YFP were incubated in 20 μM estradiol-containing liquid half-strength MS medium with 1% (w/v) Suc for 7 h. For immunoprecipitation, anti-Myc-agarose beads (Sigma-Aldrich) or GFP-Trap beads (Chromotek) were incubated

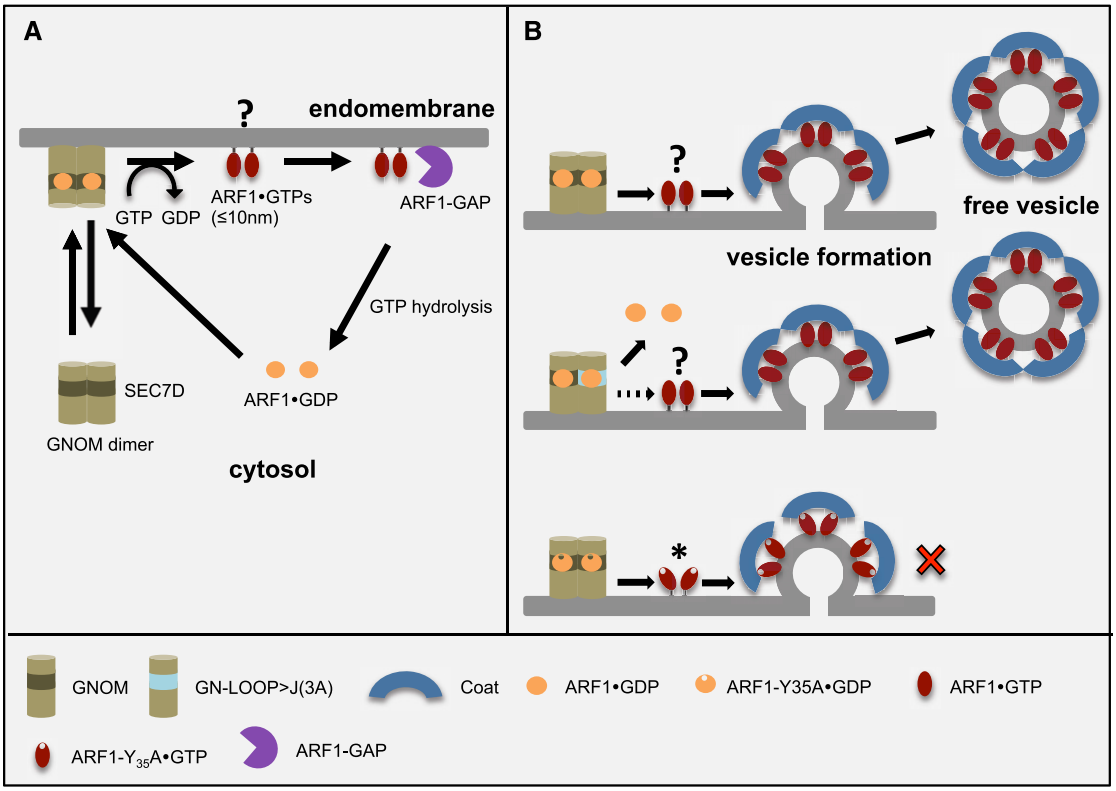

Figure 9. Close Proximity of ARF1●GTP Proteins Activated by ARF-GEF Dimers (Model).

(A) Activation-hydrolysis cycle of ARF1 GTPases. Two ARF1●GDP proteins are each simultaneously activated by membrane-associated ARF-GEF dimers, resulting in the insertion of ARF1●GTP proteins into the membrane less than 10 nm apart. GTP hydrolysis, facilitated by GTPase-activating protein (ARF1-GAP), releases ARF1●GDP proteins from the membrane back into the cytosol.

(B) Closely spaced membrane-associated ARF1●GTP proteins required for coat assembly and/or scission of membrane vesicles. In the top row, wild-type ARF-GEF dimers generate ARF1●GTPs in close proximity through simultaneous GDP-GTP exchange at the membrane. In the middle row, GN-loop>J(3A) mutant protein strongly reduces the efficiency of simultaneous ARF1 activation. Most ARF1●GDPs are immediately released into the cytosol (arrows), whereas only some are activated to form ARF1●GTPs inserted close to each other into the membrane (dashed arrow), which results in strongly reduced frequency of vesicle formation. In the bottom row, two ARF1-Y35A proteins each are coordinately activated by ARF-GEF dimers but fail to establish the close proximity of ARF1●GTP proteins required for normal coat assembly and/or vesicle scission (marked by the red X). The asterisk indicates uncertainty about the effects of the Y35A substitution in regard to hypothetical weak and transient interaction of ARF1●GTPs with each other and/or interaction with the regularly arranged coat protein complexes.

Question marks in **(A)** and **(B)** indicate uncertainty about the nature of the close spacing of ARF1●GTPs following activation by ARF-GEF dimers (e.g., hypothetical transient dimers based on weak interactions and/or stabilization by interaction with the regularly arranged coat protein complexes).

with the plant extracts at 4°C for 2.5 h. Beads were then washed two to three times with wash buffer (50 mM Tris, pH 7.5, 150 mM NaCl, and 1 mM EDTA) containing 0.1% (v/v) Triton X-100 and two to three times without Triton X-100-containing buffer. Bound proteins were eluted by boiling the beads in 2× Laemmli buffer at 95°C for 5 min. To perform immunoprecipitation in the presence of BFA, Arabidopsis seedlings were treated with 50 μM BFA for 2 h before homogenization. In addition, the same concentration of BFA was maintained during all subsequent steps of immunoprecipitation.

SDS-PAGE and Immunoblot Analysis

SDS-PAGE and immunoblotting onto PVDF membranes (Millipore) were performed as described (Lauber et al. 1997). All antibodies were diluted in 5% (w/v) milk/1× Tris-buffered saline + 0.1% (v/v) Tween 20. Antibodies and dilutions were as follows: mouse anti-c-Myc mAb 9E10 (Santa Cruz Biotechnology) 1:1000, mouse anti-GFP (Roche) 1:2500, rabbit anti-calnexin (Agrisera) 1:2000, rabbit anti-AALP (anti-aleurain; Holwerda et al., 1990 [a gift from Inhwan Hwang]) 1:1000, rabbit anti-ARF1 (Agrisera) 1:2500, rabbit anti-SEC7 (Steinmann et al., 1999) 1:2500, mouse anti-LexA (Santa Cruz Biotechnology) 1:1000, POD-conjugated anti-HA (Roche) 1:4000, anti-mouse (Sigma-Aldrich) or anti-rabbit peroxidase-conjugated (Merck Millipore) or alkaline phosphatase-conjugated antibodies (Jackson Immuno Research) 1:10,000. Detection was performed with the BM-chemiluminescence blotting substrate (Roche) and FusionFx7 imaging system (PeqLab). Image assembly was performed in Adobe Photoshop CS3, and Image Studio Lite Software (https://www.licor.com/bio/image-studio-lite/) was used for quantification of relative protein amounts.

Accession Numbers

The sequences of the genes described here can be obtained from TAIR using the following gene identifiers: *ARF1* (*ARF1A1C*; At2g47170), *GNOM* (At1g13980), and *γCOP* (At4g34450).

Supplemental Data

Supplemental Figure 1. Overview of mutant variants of ARF-GEF GNOM and ARF1 used in this study.

Supplemental Figure 2. Range of ultrastructural phenotypes of ARF1-Y35A-YFP expressing seedlings.

Supplemental Table 1. Primers used in this study.

Supplemental Table 2. Reagents, mutants and transgenic lines used.

Supplemental Data Set. Raw data and statistics of FRET-FLIM analysis presented in Figure 1E and 1F.

ACKNOWLEDGMENTS

We thank Tobias Pazen and Rebecca Stahl for technical assistance, Inwhan Hwang for providing published material, and Martin Bayer, Jeff Dangl, Christopher Grefen, Niko Geldner, and Thorsten Nürnberger for discussion and critical reading of the article. This work was supported by the Deutsche Forschungsgemeinschaft (grants Ju 179/18-1 and SFB1101/A01 to G.J. and grant SFB1101/Z02 to. Y.-D.S.) and by the Carlsberg Foundation (fellowship to M.E.N.).

AUTHOR CONTRIBUTIONS

Conceptualization: G.J.; investigation: S.B., M.K.S., M.E.N., S.R., H.B., Y.-D.S., A.-M.F., and M.K.; formal analysis: S.B.; resources: V.S.; visualization: S.B. and S.R.; project administration: S.B. and G.J.; writing original draft: G.J.; writing review and editing: S.B., M.K.S., M.E.N., S.R., H.B., Y.-D.S., A.-M.F., V.S., and G.J.; funding acquisition: G.J., M.E.N., and Y.-D.S.

Received March 25, 2020; revised May 19, 2020; accepted May 30, 2020; published June 2, 2020.

REFERENCES

Anders, N., and Jürgens, G. (2008). Large ARF guanine nucleotide exchange factors in membrane trafficking. Cell. Mol. Life Sci. **65:** 3433–3445.

Anders, N., Nielsen, M., Keicher, J., Stierhof, Y.-D., Furutani, M., Tasaka, M., Skriver, K., and Jürgens, G. (2008). Membrane association of the *Arabidopsis* ARF exchange factor GNOM involves interaction of conserved domains. Plant Cell **20:** 142–151.

Arakel, E.C., and Schwappach, B. (2018). Formation of COPI-coated vesicles at a glance. J. Cell Sci. **131:** 209890.

Beck, R., Prinz, S., Diestelkötter-Bachert, P., Röhling, S., Adolf, F., Hoehner, K., Welsch, S., Ronchi, P., Brügger, B., Briggs, J.A., and Wieland, F. (2011). Coatomer and dimeric ADP ribosylation factor 1 promote distinct steps in membrane scission. J. Cell Biol. **194:** 765–777.

Beck, R., Sun, Z., Adolf, F., Rutz, C., Bassler, J., Wild, K., Sinning, I., Hurt, E., Brügger, B., Béthune, J., and Wieland, F. (2008). Membrane curvature induced by Arf1-GTP is essential for vesicle formation. Proc. Natl. Acad. Sci. USA **105:** 11731–11736.

Bubeck, J., Scheuring, D., Hummel, E., Langhans, M., Viotti, C., Foresti, O., Denecke, J., Banfield, D.K., and Robinson, D.G. (2008). The syntaxins SYP31 and SYP81 control ER-Golgi trafficking in the plant secretory pathway. Traffic **9:** 1629–1652.

Bücherl, C.A., Bader, A., Westphal, A.H., Laptenok, S.P., and Borst, J.W. (2014). FRET-FLIM applications in plant systems. Protoplasma **251:** 383–394.

Bui, Q.T., Golinelli-Cohen, M.P., and Jackson, C.L. (2009). Large Arf1 guanine nucleotide exchange factors: Evolution, domain structure, and roles in membrane trafficking and human disease. Mol. Genet. Genomics **282:** 329–350.

Busch, M., Mayer, U., and Jürgens, G. (1996). Molecular analysis of the Arabidopsis pattern formation of gene *GNOM*: Gene structure and intragenic complementation. Mol. Gen. Genet. **250:** 681–691.

Casanova, J.E. (2007). Regulation of Arf activation: The Sec7 family of guanine nucleotide exchange factors. Traffic **8:** 1476–1485.

Dascher, C., and Balch, W.E. (1994). Dominant inhibitory mutants of ARF1 block endoplasmic reticulum to Golgi transport and trigger disassembly of the Golgi apparatus. J. Biol. Chem. **269:** 1437–1448.

Donaldson, J.G., and Jackson, C.L. (2011). ARF family G proteins and their regulators: Roles in membrane transport, development and disease. Nat. Rev. Mol. Cell Biol. **12:** 362–375.

D'Souza-Schorey, C., and Chavrier, P. (2006). ARF proteins: Roles in membrane traffic and beyond. Nat. Rev. Mol. Cell Biol. **7:** 347–358.

Fäßler, F., and Pimpl, P. (2017). In vivo interaction studies by measuring Förster resonance energy transfer through fluorescence lifetime imaging microscopy (FRET/FLIM). Methods Mol. Biol. **1662:** 159–170.

Geldner, N., Anders, N., Wolters, H., Keicher, J., Kornberger, W., Muller, P., Delbarre, A., Ueda, T., Nakano, A., and Jürgens, G. (2003). The Arabidopsis GNOM ARF-GEF mediates endosomal recycling, auxin transport, and auxin-dependent plant growth. Cell **112:** 219–230.

Geldner, N., Richter, S., Vieten, A., Marquardt, S., Torres-Ruiz, R.A., Mayer, U., and Jürgens, G. (2004). Partial loss-of-function alleles reveal a role for *GNOM* in auxin transport-related, post-embryonic development of *Arabidopsis*. Development **131:** 389–400.

Gillingham, A.K., and Munro, S. (2007). The small G proteins of the Arf family and their regulators. Annu. Rev. Cell Dev. Biol. **23:** 579–611.

Grebe, M., Gadea, J., Steinmann, T., Kientz, M., Rahfeld, J.-U., Salchert, K., Koncz, C., and Jürgens, G. (2000). A conserved domain of the *Arabidopsis* GNOM protein mediates subunit interaction and cyclophilin 5 binding. Plant Cell **12:** 343–356.

Holwerda, B.C., Galvin, N.J., Baranski, T.J., and Rogers, J.C. (1990). In vitro processing of aleurain, a barley vacuolar thiol protease. Plant Cell **2:** 1091–1106.

Huang, L., Franklin, A.E., and Hoffman, N.E. (1993). Primary structure and characterization of an *Arabidopsis thaliana* calnexin-like protein. J. Biol. Chem. **268:** 6560–6566.

Kumaran, M., Ye, D., Yang, W.-C., and Sundaresan, V. (1999). The DIRECTIONLESS mutation affects the pattern formation in Arabidopsis. 10th International Conference on Arabidopsis Research, Melbourne, Australia. Abstract: 8–24.

Künzl, F., Früholz, S., Fäßler, F., Li, B., and Pimpl, P. (2016). Receptor-mediated sorting of soluble vacuolar proteins ends at the trans-Golgi network/early endosome. Nat. Plants **2:** 16017.

Lauber, M.H., Waizenegger, I., Steinmann, T., Schwarz, H., Mayer, U., Hwang, I., Lukowitz, W., and Jürgens, G. (1997). The Arabidopsis KNOLLE protein is a cytokinesis-specific syntaxin. J. Cell Biol. **139:** 1485–1493.

Lowery, J., et al. (2011). Novel C-terminal motif within Sec7 domain of guanine nucleotide exchange factors regulates ADP-ribosylation factor (ARF) binding and activation. J. Biol. Chem. **286:** 36898–36906.

Mehlhorn, D.G., Wallmeroth, N., Berendzen, K.W., and Grefen, C. (2018). 2in1 vectors improve in planta BiFC and FRET analyses. Methods Mol. Biol. **1691:** 139–158.

Mossessova, E., Corpina, R.A., and Goldberg, J. (2003). Crystal structure of ARF1*Sec7 complexed with brefeldin A and its implications for the guanine nucleotide exchange mechanism. Mol. Cell **12:** 1403–1411.

Müller, A., Guan, C., Gälweiler, L., Tänzler, P., Huijser, P., Marchant, A., Parry, G., Bennett, M., Wisman, E., and Palme, K. (1998). AtPIN2 defines a locus of Arabidopsis for root gravitropism control. EMBO J. **17:** 6903–6911.

Peyroche, A., Antonny, B., Robineau, S., Acker, J., Cherfils, J., and Jackson, C.L. (1999). Brefeldin A acts to stabilize an abortive ARF-GDP-Sec7 domain protein complex: Involvement of specific residues of the Sec7 domain. Mol. Cell **3:** 275–285.

Ramaen, O., Joubert, A., Simister, P., Belgareh-Touzé, N., Olivares-Sanchez, M.C., Zeeh, J.C., Chantalat, S., Golinelli-Cohen, M.P., Jackson, C.L., Biou, V., and Cherfils, J. (2007). Interactions between conserved domains within homodimers in the BIG1, BIG2, and GBF1 Arf guanine nucleotide exchange factors. J. Biol. Chem. **282:** 28834–28842.

Renault, L., Guibert, B., and Cherfils, J. (2003). Structural snapshots of the mechanism and inhibition of a guanine nucleotide exchange factor. Nature **426:** 525–530.

Robineau, S., Chabre, M., and Antonny, B. (2000). Binding site of brefeldin A at the interface between the small G protein ADP-ribosylation factor 1 (ARF1) and the nucleotide-exchange factor Sec7 domain. Proc. Natl. Acad. Sci. USA **97:** 9913–9918.

Singh, M.K., and Jürgens, G. (2018). Specificity of plant membrane trafficking: ARFs, regulators and coat proteins. Semin. Cell Dev. Biol. **80:** 85–93.

Singh, M.K., Krüger, F., Beckmann, H., Brumm, S., Vermeer, J.E.M., Munnik, T., Mayer, U., Stierhof, Y.D., Grefen, C., Schumacher, K., and Jürgens, G. (2014). Protein delivery to vacuole requires SAND protein-dependent Rab GTPase conversion for MVB-vacuole fusion. Curr. Biol. **24:** 1383–1389.

Singh, M.K., et al. (2018). A single class of ARF GTPase activated by several pathway-specific ARF-GEFs regulates essential membrane traffic in Arabidopsis. PLoS Genet. **14:** e1007795.

Spitzer, M., Wildenhain, J., Rappsilber, J., and Tyers, M. (2014). BoxPlotR: A web tool for generation of box plots. Nat. Methods **11:** 121–122.

Steinmann, T., Geldner, N., Grebe, M., Mangold, S., Jackson, C.L., Paris, S., Gälweiler, L., Palme, K., and Jürgens, G. (1999). Coordinated polar localization of auxin efflux carrier PIN1 by GNOM ARF GEF. Science **286:** 316–318.